A high-performance elastomeric patch clamp chip†‡

Chihchen Chen and Albert Folch*

Received 5th June 2006, Accepted 3rd August 2006
First published as an Advance Article on the web 23rd August 2006
DOI: 10.1039/b607913j

Ion channels play key roles in cell physiology and underlie a broad spectrum of disorders. To this day, the gold standard for studying ion channels is the patch clamp technique. Patch clamping involves careful positioning of a fine-tipped glass micropipette onto the surface of the cell to form a high-resistance (>1 GΩ) seal (''gigaseal''), a procedure that is laborious, vibration-sensitive, and not easily amenable to automation. In addition, the solution inside the pipette cannot be easily exchanged. Recently reported patch clamp chips offer the potential of increased throughput, but to date the overall per-cell performance of most designs has been very low when compared to pipettes, and/or the fabrication process is prohibitively expensive. Here we demonstrate a replica-molded elastomeric patch clamp chip incorporating nanofabricated constrictions, which delivers high-stability gigaseals, with success rates comparable to those of pipettes, using rat basophilic leukemia (RBL) cells. The high stability enables exchanges of both the extracellular and intracellular solution during whole-cell recordings. In a sample of 103 experiments, 66 cells (64%) were successfully immobilized at the patch aperture; 38 cells (58% of immobilized cells, 37% of all cells) were successfully gigasealed; and 25 cells (65% of gigasealed cells, 34% of immobilized cells, 24% of all cells) were successfully perforated for whole-cell access. In the last group of 27 experiments, 79% of the cells could be immobilized, of which 68% could be gigasealed and 46% perforated for whole-cell access, indicating that dexterity is important.

Introduction

Patch-clamp technology has revolutionized basic neuroscience research by enabling the functional characterization of ion channel function with high information content and temporal resolution[1–4] (see review[5]). Unfortunately, present pipette-based technology suffers from several critical drawbacks: it requires (a) costly micropositioning hardware that is delicate and cumbersome (can interfere with perfusion or microscope setups); (b) non-portable fluidic handling setups; (c) fine manual dexterity; and (d) lengthy preparation. All steps are normally performed manually. In addition, it is difficult to exchange the solution inside the micropipette. As a result, pipette-based technology cannot be scaled up to provide the throughput necessary for efficient screening in the drug discovery process. As a higher-throughput alternative to patch clamp micropipettes, several groups have developed patch clamp chips that feature a microaperture onto which the cells are positioned in a semi-automated way.

Many strategies have been investigated to fabricate planar apertures (*i.e.* the aperture is on a flat surface) using either glass,[6–10] silicon,[11–16] or elastomeric[17–19] substrates. Some commercial products for high-throughput electrophysiology such as the SealChip™[20] do not disclose the fabrication process or the gigaohm-seal (''gigaseal'') yields and are sold only as part of expensive equipment packages. The silicon-based Qpatch™[21] advertises high yields (63% gigaseal success using HEK, CHO and RBL cell lines, n = 141).[22] One major disadvantage of glass or quartz chips is the high processing costs, especially because defining the aperture involves equipment that is prohibitively expensive, proprietary, and/or not readily available to most researchers. Silicon-based devices, albeit cheaper, feature large capacitances (tens to hundreds of picofarads) between the aqueous solutions and the bulk silicon;[23] these values are much larger than those obtained with a traditional micropipette, impairing the signal-to-noise ratios even if gigaseals were to form. Several groups have explored the use of poly(dimethylsiloxane) (PDMS) for making patch clamp chips. PDMS (also known as Sylgard 184 from Dow Corning) is an attractive material because it can be molded inexpensively with high fidelity and has a low dielectric constant. However, PDMS chips featuring planar apertures have only produced low yields (<10% gigaseal success rates) so far.[18,19] Importantly, the fluidic connection to the aperture interferes with the light path in phase-contrast microscopy, producing blurry images.[24]

Recently, Lee and colleagues have reported that, surprisingly, good seals can be formed using a ''cornered'' (non-planar) aperture (*i.e.* a microchannel opening 4 μm × 3 μm in size).[25,26] Cornered apertures are straightforward to mold in PDMS, are readily connected to a fluidic inlet *via* a microchannel, and are compatible with phase-contrast imaging;

Department of Bioengineering, University of Washington, Seattle, Washington, 98195, USA. E-mail: afolch@u.washington.edu

† Electronic supplementary information (ESI) available: Supplementary movie. Microfluidic exchange of the extracellular solution (ECS). Movie illustrating an ECS exchange with red and green dye solutions. Fluid flows through both nCh_{EC} towards the inlet of μCh_{in}, resulting in a laminar stream boundary that can be steered by changing the flow rates through either nCh_{EC}. See DOI: 10.1039/b607913j

‡ The HTML version of this paper has been enhanced with additional colour images.

gigaseals could be obtained on CHO cells expressing outward-rectifying Kv2.1 channels, albeit in very low yields (5% of all cells; 73% of the seals were lower than 250 MΩ).[26] Here we report in detail the performance of a modified cornered-aperture design that fares well *when compared to micropipettes*. Our device incorporates several nanofabricated channels that we believe play a key role in improving the yields dramatically. The devices are designed to record from only one cell in order to focus on the fundamentals of gigaseal quality without the complications that can arise from multiple/simultaneous recordings. In order to obtain reliable statistics on the high performance of the device, we gathered gigaseal-attempt data from 103 devices and each device was only used once.

Experimental

Patch clamp chip fabrication

The mold is microfabricated in the photoresist SU-8 (Microchem Inc., Newton, MA, USA) using a conventional two-layer lithography process. Conveniently, SU-8 is cross-linked both by UV light and electron-beam radiation. First, a ~1 μm-wide line and six ~5 μm-wide lines (see pattern in Fig. 1a) are drawn on a ~1 μm thick layer of SU-8-2 using electron-beam writing. Second, the pattern is coated with a 20 μm thick layer of SU-8-2035 and exposed to UV light (following Microchem's specifications) through a high-resolution transparency photomask (20 000 dpi printing resolution, CAD/Art Services, San Diego, CA, USA) containing a pattern of 50–100 μm-wide lines, which is aligned with the previous e-beam pattern. Developing the SU-8 resists reveals a set of thick lines (50 μm × 20 μm smallest cross section) and a set of thin lines (1 μm × 1 μm smallest cross section) connected with each other (Fig. 1b). The master is then exposed to an O_2 plasma (Branson; parameters: 1 Torr, 300 W, 2 min) to smoothen the microscale features of the photoresist. A base and a curing agent of PDMS are mixed (1 : 10 wt/wt) and the liquid mixture is poured onto the mold and cured at 65 °C for at least overnight. The cured PDMS replica is peeled off the SU-8 mold and bonded to a ~0.5 mm thick PDMS layer after an O_2 plasma treatment (0.7 Torr, 100 W, 10 s) (Fig. 1c).

Cell culture

The RBL cell line was purchased from ATCC (CRL no. 1378, American Type Culture Collection, Manassas, VA, USA). The cells were cultured in DMEM (Gibco, Grand Island, NY, USA) supplemented with 10% (v/v) FBS, penicillin (100 units mL^{-1}), and streptomycin (100 μg mL^{-1}) and maintained at 37 °C under a humidified atmosphere at 5% CO_2 and 95% air. The cell culture was maintained between 1×10^5 and 1×10^6 cells mL^{-1} by addition of or replacement of cells by fresh medium. The cells were thawed according to ATCC's protocol, except that after ~5 h the cells were centrifuged and re-suspended in fresh medium to remove residual DMSO (present in ATCC's frozen pellet). Typically, ~10–15 days of continuous culture was necessary before obtaining a "good" culture; a culture was deemed "good" when it had (a) the correct density (between 10^5 and 10^6 cells mL^{-1}), (b) few dead cells, (c) no clumps of cells, and (d) most cells looking

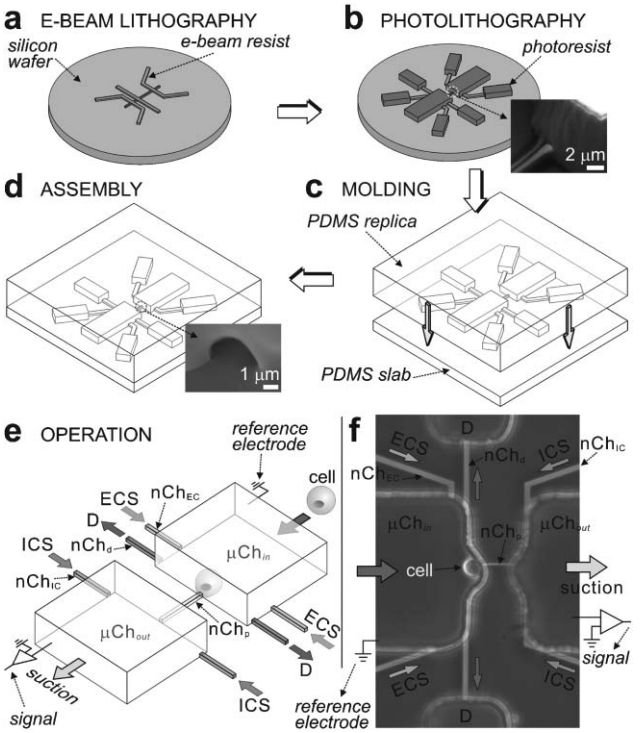

Fig. 1 Fabrication and operation of the PDMS patch-clamp chip. A master mold is made by (a) electron-beam lithography (line thickness: 1 μm, line width: 1 or 5 μm, see text) and (b) subsequent conventional photolithography (20 μm thick, 100 μm wide); the inset is an SEM image that shows where the electron-beam resist pattern meets the photoresist pattern. (c and d) A PDMS replica is cast and chemically bonded to a thin (~0.5 mm thick) PDMS slab; the inset is an SEM image that shows the nanochannel opening as seen from the microchannel. (e) Schematic rendition and (f) phase-contrast micrograph of the device; the cell is loaded into a microchannel (μCh_{in}) and immobilized at the opening of the probing nanochannel (nCh_p, connected to the signal electrode through μCh_{out}). During the cell immobilization procedure, fluid is ejected from nCh_p (against the μCh_{in} flow) to keep the nCh_p opening clean, so that flow goes into the drain (D) nanochannel (nCh_d). After cell immobilization, suction is applied to μCh_{out} to obtain a gigaseal; whole-cell access is obtained with a further increase in suction. Different extracellular (ECS) and intracellular (ICS) solutions can be introduced into μCh_{in} through nCh_{EC} and into μCh_{out} through nCh_{IC}, respectively.

"healthy" (*i.e.* round, bright, and containing few black granules inside) in phase-contrast microscopy.

Solutions

All chemicals were obtained from Sigma–Aldrich. The intracellular solution consisted of (in mM) 145 KCl, 8 NaCl, 1 $MgCl_2$, 10 EGTA, 10 HEPES, and 2 Mg–ATP,[27] titrated to pH 7.2 with KOH. This solution was stored at −20 °C. Since magnesium ions form complexes with compounds such as ATP, EGTA, and EDTA, for experiments where the concentration of magnesium ions ($[Mg^{2+}]$) was important we estimated the free $[Mg^{2+}]$ using a program (WinMaxc32 v2.50, http://www.stanford.edu/~cpatton/downloads.htm) that takes into account the dissociation constants of Mg^{2+}-complexing compounds. The free $[Mg^{2+}]$ was estimated as 0.8 mM for the regular intracellular solution. The "Mg^{2+}-free" solution had

no added Mg^{2+} and Mg–ATP was replaced by 4 mM K_2ATP, resulting in an estimated free [Mg^{2+}] of 0.19 μM (for a trace total [Mg^{2+}] = 15 μM; 1 mM EDTA was added for some experiments). The extracellular solution contained (in mM) 145 NaCl, 2.8 KCl, 2 $MgCl_2$, 10 $CaCl_2$, 10 HEPES, and 10 glucose,[27] adjusted to pH 7.2 with NaOH. This solution was stored at 4 °C. In some experiments, the extracellular solution contained different K^+ concentrations (the sum of [Na^+] and [K^+] was kept constant).

Patch-clamp chip recordings

Experiments were done in whole-cell configuration of the patch-clamp technique.[1,5] All experiments were performed at room temperature (19–22 °C). We evaluated 103 devices, and each device was used only once (*i.e.* cells always contacted an aperture that had never been contacted by a cell before). Before an experiment, patch-clamp chips were O_2 plasma-treated (100 W, 0.7 Torr, 6 min) to render the microchannel surfaces hydrophilic (the O_2 plasma penetrates into the channels through the inlets), then immediately filled with electrolytic solutions and used within 5 h. The patch-clamp amplifier (Multiclamp 700A; Axon Instruments Inc., CA, USA) was used in the voltage-clamp mode with series resistance compensation. The command input of the Multiclamp 700A was controlled by a computer *via* a digital-analog converter in a data acquisition system (Digidata 1322, Axon Instruments Inc., CA, USA), which also sampled the low-pass filtered clamping current simultaneously. The voltage was set to a "holding" potential of −60 mV prior to obtaining *I–V* curves. Steady-state currents were always taken as the mean value during the last 50 ms of a 200 ms voltage pulse (starting at −140 mV and finishing at +80 mV in 10 mV increments). The data were filtered at 4.5 kHz with an eight-pole Bessel filter, digitized at 10 kHz. Before applying the test-pulse sequences, capacitance was automatically compensated with two variable capacitors in the Multiclamp 700A. Unless indicated, recordings were post-processed with leak subtraction.

Pipette-based patch clamp recordings

Autoclaved glass cover slips were coated with poly-D-lysine (PDL) as a cell adhesion promoter. The PDL solution (10–100 μg mL^{-1}) was added to the cover slips and aspirated after 1 h. Next, the PDL-coated cover slips were washed three times with autoclaved filtered water, air-dried, and stored for 12 h before usage. RBL cells were seeded on the PDL-coated cover slips one day before electrophysiological recordings. Electrodes pulled from borosilicate glass micropipette tubes (Sutter Instruments) had intrinsic resistances of 4.5 ± 1.5 MΩ (33% variability) and non-optimized capacitances of ~1.5 pF (slightly lower values can be obtained by minimizing the fluid above the cell and by coating the pipette with low dielectric constant materials).

Results and discussion

Device design

The device is fabricated in poly(dimethylsiloxane) (PDMS) by replica-molding from a microfabricated master as schematically depicted in Fig. 1a–d. The master mold contains small, nanofabricated features (one ~1 μm wide line and six ~5 μm wide lines, ~1 μm thick) defined by electron-beam lithography (Fig. 1a) and overlapping large features (~50–100 μm wide, ~20 μm thick) defined by standard photolithography (Fig. 1b) (see Experimental). Shown in the inset of Fig. 1b is a scanning electron micrograph (SEM) of the mold at the point where a small line meets a large line. A PDMS replica of the master (Fig. 1c) is bonded against a ~0.5 mm thick PDMS slab (Fig. 1d) following standard soft lithography procedures.[28] The replicas of the lines in the master now form channels in PDMS. The inset in Fig. 1d shows an SEM image of the aperture formed at the junction between the small and large channels. To distinguish them, we term the large channels "microchannels" (μCh) and the smaller ones "nanochannels" (nCh). (Thus, here "nano" signifies "nanofabricated" rather than the more usual meaning "nanoscale"; while the nanochannels are not submicron in scale, submicron-resolution ("nano") lithography is required to precisely define them.)

Device operation

The schematic in Fig. 1e and the micrograph in Fig. 1f illustrate the operation of the device. The cells are loaded through an "input microchannel" (μCh_{in}, connected to the reference electrode), which communicates with an "output microchannel" (μCh_{out}, connected to the signal electrode). The μCh_{in} and the μCh_{out} are communicated *via* a ~30 μm long nanochannel, termed the "probe nanochannel" (nCh_p). The μCh_{in} is filled with extracellular solution (ECS) and the μCh_{out} is filled with intracellular solution (ICS). Both ECS and ICS can be exchanged *via* two pairs of independent nanochannels, termed nCh_{EC} and nCh_{IC}, respectively, which are connected to μCh_{in} and μCh_{out}, respectively. Cells in suspension are collected and washed twice with extracellular solution to remove proteins and debris in the culture medium. After injecting the cell suspension (2 μL, ~5×10^5 cells mL^{-1}) into the inlet of the μCh_{in}, cells are driven by flow until one of them blocks the opening of the nCh_p, similarly to the method by Ionescu-Zanetti *et al.*,[26] thus eliminating the micropositioning typical of pipette-based recordings. At the same time, and crucially important, a positive pressure is applied to the μCh_{out} in order to keep the opening of the nCh_p clean while the cell is approaching the nCh_p opening. A set of "drain nanochannels" (nCh_d) allows fluid to escape while positive pressures are applied to both μCh_{in} and μCh_{out}. The typical pressure used by hand to drive the flow is ~0.5–1 kPa (as measured by the rise in height of a water column connected to the microchannel). This pressure range ensures reasonable sealing between the cell membrane and the nCh_p walls without inducing mechanical damage to the cell membrane. Both positive pressures are switched off once a cell is captured. Next, gentle suction is applied by hand to μCh_{out} to facilitate the formation of a gigaseal and turned off once the gigaseal is obtained. After the seal is stable, application of a sudden increase in suction results in electrical access to the cell's interior ("whole-cell access"). Suction application procedures are identical to those used to apply suction in pipette-based recordings.

Whole-cell recordings

Our rationale for incorporating nanochannels in our design was that the high fluidic resistance of the nanochannels would reduce the stringent requirements for user dexterity in applying pressures during operation as encountered in pipette-based recordings. To test the device's performance, we performed whole-cell recordings from RBL cells expressing endogenous inward-rectifier potassium channels ("K_{ir} channels") as a model of electrophysiological studies. In brief, signal quality was indistinguishable from that obtained with a pipette. In all recordings the gigaseal was stable for *at least* 10 min; this 10 min duration likely does not reflect a feature of the device but simply the fundamental "endurance" of the cell as its contents are free to diffuse out.

Fig. 2a shows the applied 10 mV increment, 200 ms duration voltage pulses (top) and a representative example of the evoked whole-cell currents measured with the chips (bottom). The strong inward rectification typical of K_{ir} channels is manifested in the very small currents (<0.01 nA) recorded above E_K, the calculated Nernst potential for K^+ (see below for measurements of E_K), as expected from theoretical considerations and past studies.[5] Fig. 2b shows the steady-state current–voltage (*I–V*) plot of the data in Fig. 2a and the leak-subtracted values. Similar curves obtained with pipettes are indistinguishable from these in amount of noise and leak resistances measured. The intrinsic capacitance of the devices ranges from 0.8 pF (if nCh_{EC} and nCh_{IC} are empty) to 1.3 pF (if nCh_{EC} and nCh_{IC} are filled), which compares well with pipettes; bare glass pipettes have capacitances of ~0.4–1.25 pF per millimeter immersed in the cell culture bath,[29] so capacitances >1 pF are common.

We evaluated a large number of devices (n = 103) to extract statistically-valid conclusions on device performance. For consistency, devices were never re-used, *i.e.* the cells always arrived at an aperture that had never been contacted by a cell before. Fig. 2c summarizes the success rates at each step of whole-cell recordings. Cells were scored as having formed a gigaseal only if the seal resistance prior to attempting whole-cell access (R_{seal}) was >1 GΩ. The overall success rates of cell immobilization at the nCh_p opening, formation of gigaseals, and whole-cell access were respectively 59% (n = 44), 31% (n = 23), and 20% (n = 15) for the first 75 experiments (n = 1–75) and rose to 79% (n = 22), 54% (n = 15), and 36% (n = 10) for the last 28 experiments (n = 76–103), likely due to improved dexterity. Amongst the cells that were successfully immobilized to the nCh_p opening (n = 66; n = 44 for low dexterity and n = 22 for high dexterity), gigaseals were obtained on 23/44 = 52% (low dexterity) to 15/22 = 68% (high dexterity) of the cells. Amongst all the cells that were successfully "gigasealed" (n = 38; n = 23 for low dexterity and n = 15 for high dexterity), whole-cell access was achieved with the same success for low and high dexterity (15/23 = 65% and 10/15 = 67%, respectively), indicating that dexterity is not important for gaining whole-cell access once the cell has been gigasealed.

There does not appear to be any correlation between R_{seal} and the resistance before cell contact ("intrinsic resistance" R_i), as shown in the Fig. 2d plot including all the cells that were successfully immobilized (n = 66). Importantly, all the cells

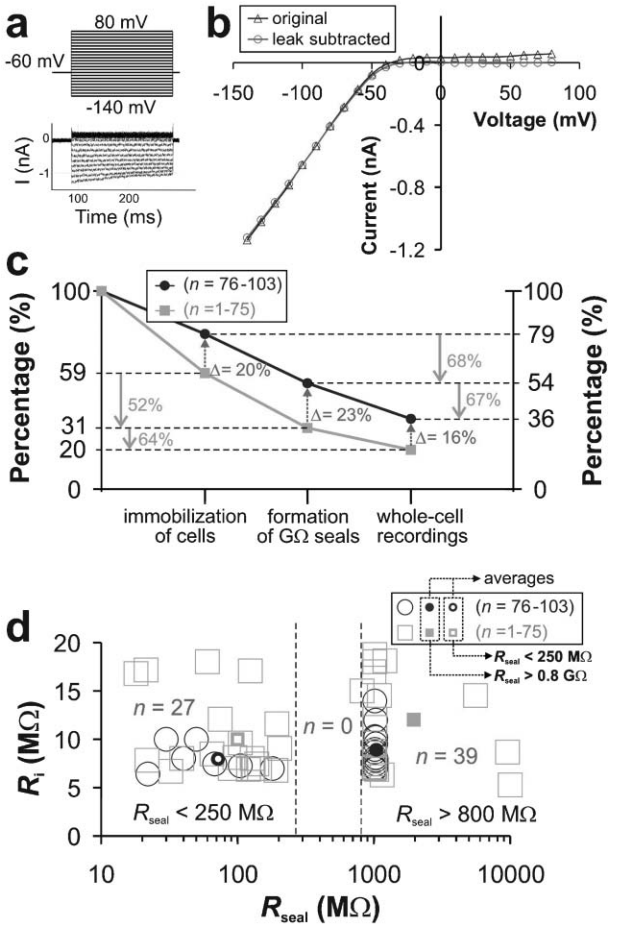

Fig. 2 Whole-cell recordings by using the PDMS patch-clamp chip. (a) Representative whole-cell currents (*I*) obtained with the PDMS patch-clamp chip (*bottom*) in response to voltage steps of 200 ms duration and between −140 mV to +80 mV in 10 mV increments from a holding potential of −60 mV (*top*). (b) Steady-state *I–V* curve; the original data (*triangles*) is linear fitted from 0 mV to 80 mV to find a "leak" resistance of 3.15 GΩ, which can be subtracted (*circles*). (c) Success rates at each step of whole-cell recordings; over n = 103 experiments, the success rates increase in the last 28 experiments due to improved dexterity with respect to the first 75 experiments. (d) Plot of intrinsic resistance (R_i) *versus* resistance prior to attempting whole-cell access (R_{seal}) for the n = 66 cells that were successfully immobilized. Of these, 27 cells (41%) failed to form a high seal resistance while 38 cells (59%) gigasealed. Note the absence of R_{seal} values between 250 MΩ and 800 MΩ. The low-dexterity (n = 1–75, *squares*) and high-dexterity (n = 76–103, *circles*) groups of experiments do not differ substantially in the average R_{seal} values and only slightly in the average R_i values for both R_{seal} < 250 MΩ (*thick squares* and *thick circles*, respectively) and R_{seal} > 800 MΩ (*filled squares* and *filled circles*, respectively) data ranges.

that were immobilized but not gigasealed displayed R_{seal} values < 250 MΩ (41%), *i.e.* we have never observed intermediate R_{seal} values (250 MΩ < R_{seal} < 800 MΩ; only 1 cell in the range 800 MΩ < R_{seal} < 1 GΩ). Interestingly, dexterity affects the gigaseal success rate but not the actual R_{seal} values (see Fig. 2d), indicating that the seal is a fundamental/compounded property of the device and/or the cells. On the other hand, dexterity has a small effect on the obtained R_i values, perhaps stressing the influence of dexterity on the immobilization

procedure. The best gigaseals always appear to form spontaneously (or with brief, little suction) upon immobilization to the nCh_p opening, and we have rarely obtained a gigaseal on second attempt, *i.e.* by applying repetitive or continuous suction. This observation is universally common with pipettes as well, suggesting that a low R_{seal} and a gigaseal are two fundamentally different types of seals: a low R_{seal} simply reflects the occlusion of the fluid channel by the cell, whereas a gigaseal reflects the occurrence of an intimate contact between the cell membrane and the PDMS surface. Low R_{seal} is often observed in circumstances that could potentially be avoided, such as those involving (a) cell cultures that show abnormal cell morphology (see Experimental for our assessment of "good" cultures), (b) cells that have been pushed too hard against the aperture, and/or (c) solutions containing debris (that presumably obstruct or contaminate the aperture). In general, our yields suffer from the same critical dependence on cell preparation as micropipette recordings (see below), indicating that the cell type and preparation pose more fundamental limits on the ultimate yield than the dexterity or than the device itself.

Similarly, Klemic *et al.*[19] have reported that some days the gigaseal success (evaluated with *Xenopus* oocytes and CHO or RBL cells in planar-aperture PDMS patch-clamp chips) was higher than other days.

Small topological differences could be responsible for the improvement over previous reports that used a cornered-aperture PDMS design,[26] in particular our method for defining the nanochannels by means of electron beam lithography which provides higher resolution for making smaller apertures. High-resolution photomasks are indispensable for producing microchannels with smooth sidewalls. We failed to obtain gigaseals from devices made with transparency photomasks of 3600 dpi resolution in earlier experiments. In addition, we only obtain gigaseals if the masters have been exposed to O_2 plasma, a process that etches and heats up the mold, both of which contribute to smoothen the roughness of the mold (see inset in Fig. 1a). We have also observed that (but have not been able to elucidate why) a particular master mold yields lower R_i than the others, suggesting that small geometrical differences in the resolution of the lines and/or the micro-aperture could be critical. For example, for all devices ($n = 103$) from all molds, $R_i = 10.5 \pm 4.6$ MΩ (44% variability) but for one given mold the standard deviation could be lower, *e.g.* $R_i = 8.99 \pm 2.63$ MΩ (29% variability, $n = 47$), suggesting that part of the variability is due to the device and part is due to other factors such as small inconsistencies in the fluid handling protocol. (With a different, silicon-based chip design and CHO-K1 cells, Pantoja *et al.*[15] similarly observed that R_{seal} values were different for two different fabrication runs.) By comparison, we have observed that an automated pipette puller (see Experimental) yields even higher variability from day to day in our laboratory. We expect that a survey and inspection of many different molds will shed light over the optimal microscale geometries.

Klemic *et al.*[19] have reported that 1–4 h of O_2 plasma treatment of PDMS devices improves the rate of gigaseal formation. We do not obtain gigaseals without O_2 plasma treatment, either. However, with our O_2 plasma apparatus, the optimal duration is 6 minutes in the tested range of 0 to 9 minutes; more prolonged exposures to O_2 plasma do not improve gigaseal formation rates and introduce cracks on the PDMS surface, which deteriorate the imaging quality of phase-contrast microscopy. Once treated, the devices are immediately filled with electrolytic solutions and used within 5 h. We have not investigated the shelf life of our devices after performing O_2 plasma. Ionescu-Zanetti *et al.*[19] have used partial curing bonding of PDMS to improve the seal resistance without the use of O_2 plasma.

A "shopping comparison" between the various patch clamp chip designs is difficult because success rates are highly dependent on cell type (as is widely known for pipette-based recordings) and some fabrication parameters such as O_2 plasma exposure that are not easily translated to other laboratories; furthermore, most studies (including ours) limit their scope to one cell type for simplicity. Using a PDMS cornered-microaperture patch clamp chip, Ionescu-Zanetti *et al.*[26] have reported success rates of gigaseals of 5% on CHO cells expressing outward rectifying Kv2.1 channels (the number of devices evaluated was small and the success rates of whole-cell access or seal stabilities were not reported); by comparison, typical gigaseal success rates on CHO cells using micropipettes can reach 95%.[30] The commercial, silicon-based Qpatch™ system[21] advertises 63% gigaseal yields using HEK, CHO and RBL cell lines,[22] but the design details are not revealed. An ongoing survey of a variety of cell types with our chip should reveal whether the performance of our design is specific to the RBL cell type or intrinsically superior.

Extracellular perfusion

The microfluidic architecture of the device, combined with the high stability of the gigaseal, allows for alternatively injecting two different ECS through dedicated nCh_{EC} without disrupting the gigaseal. The junction between the nCh_{EC} and the μCh_{in} is only within a few microns of the cell so that the dead volume is very small. Small dead volumes are important because in microchannels fluids flow laminarly (*i.e.* without turbulence[31]) and close to the walls the fluid velocity is essentially zero,[31] so complete removal of ECS around the cell can only occur by diffusion; since the diffusion time scales as the square of the diffusion distance,[31] there is great advantage in keeping the volumes small for fast solution exchanges. To exchange the ECS, both nCh_{EC} are positively pressurized (with syringe pumps), resulting in two laminar-flow streams flowing back towards the inlet of the μCh_{in}; a demonstration with dyes is shown in Fig. 3a and in the Supplementary movie.† The width of each stream depends on the flow rates injected into the two nCh_{EC}, so by adjusting the flow rates one stream can fill most of the channel (enveloping the cell) and be quickly retracted within a fraction of a second.

Whole-cell *I–V* curves during extracellular perfusion are shown in Fig. 3b. Here, the cell is voltage-clamped at −60 mV and perfused with ECS of different extracellular K^+ concentration ($[K^+]_o$; the change in K^+ ions is compensated with the same amount of Na^+ ions added in the ECS to preserve osmolarity). At all $[K^+]_o$ tested, cells display the typical rectifier behavior. When $[K^+]_o$ is increased from 2.8 mM to

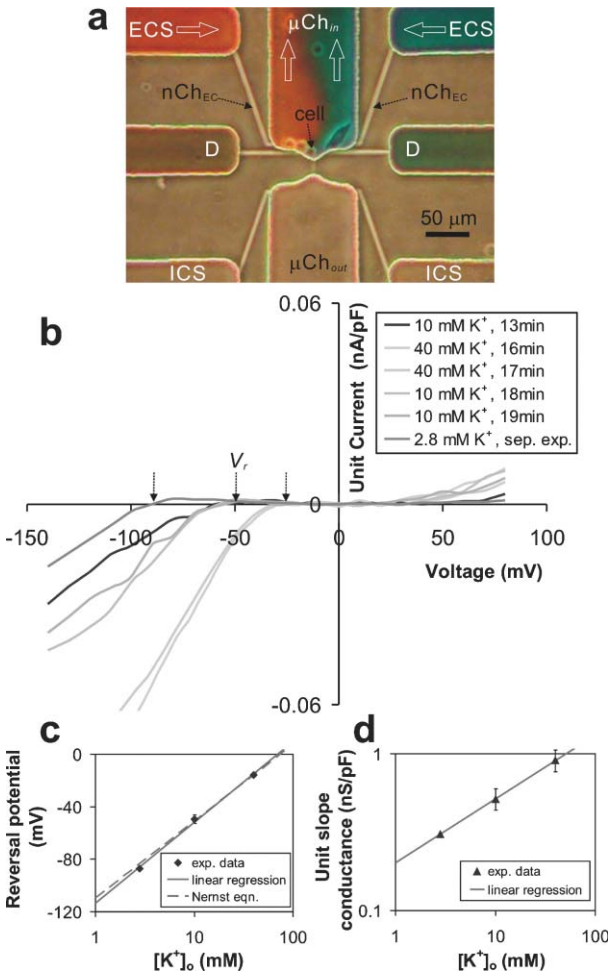

Fig. 3 Microfluidic exchange of the extracellular solution (ECS). (a) Optical micrograph of the device illustrating an ECS exchange with dye solutions. Fluid flows through both nCh_{EC} towards the inlet of μCh_{in} (see arrows indicating flow direction), resulting in a laminar stream boundary that can be steered by changing the flow rates through either nCh_{EC}. (b) Steady-state *I–V* curves for different extracellular potassium ($[K^+]_o$) concentrations introduced into μCh_{in} through the two nCh_{EC}. The sum $[K^+]_o + [Na^+]_o$ was kept constant (147.8 mM). Data were obtained from recordings on the same cell except data at $[K^+]_o$ = 2.8 mM. One of the nCh_{EC} was used to introduce $[K^+]_o$ = 10 mM and the other to introduce $[K^+]_o$ = 40 mM in ~1 min intervals. Zero-current (rectification) potentials V_r are indicated by the arrows. (c) V_r as a function of $[K^+]_o$ (logarithmic scale). The solid line is a linear regression fit (r^2 = 0.997) to the data and the dashed line is the potential predicted by the Nernst equation. (d) Double-logarithmic plot of unit-slope conductance (linear-regression slope of *I–V* curves between −120 mV and −80 mV normalized to whole-cell capacitance, r^2 = 0.993) *versus* $[K^+]_o$. The solid line is a linear regression fit (r^2 = 0.993) to the data.

10 mM and 40 mM, the rectification voltage (V_r) shifts to more positive potentials from −87.3 mV to −49.5 mV and −16.0 mV, respectively. For all the cells tested, the direction of the shift parallels the change in the Nernst potential for K^+ (E_K), *i.e.* $V_r \sim E_K$, as expected[5]. The linear fit of V_r is 61.7 log $[K^+]_o$ − 113.6 (correlation coefficient r^2 = 0.997), in very good (~5%) agreement with the Nernst equation (E_K = 58.67 log $[K^+]_o$ − 109.6), as shown in Fig. 3c. We also studied the "unit-slope" conductance *G* (the slope of the linear fit of steady-state *I–V* curves between −120 mV and −80 mV, divided by the whole-cell capacitance to normalize for differences in size between cells from different experiments). For the $[K^+]_o$ values examined (2.8 mM, 10 mM and 40 mM), *G* is 0.45 $nSpF^{-1}$, 0.69 nS pF^{-1}, and 1.28 nS pF^{-1}, respectively. These values fit a dependence $G = 0.3\ ([K^+]_o)^{0.39}$ (r^2 = 0.993) (Fig. 3d), in very good agreement with results obtained for inward rectifiers in other cells ($G \sim [K^+]_o)^{0.5}$) (see refs. 32,33) and with the model by Hille and Schwarz ($G \sim [K^+]_o)^{0.4}$) (see ref. 34).

Intracellular solution exchanges

A unique feature of our design is that exchanges of ICS in the μCh_{out} through the two nCh_{IC} channels is also possible without disrupting the gigaseal. As demonstrated with dyes in Fig. 4a, the procedure for exchanging the ICS in the μCh_{out} is identical to that for exchanging ECS in the μCh_{in} (described above); for ICS exchanges the dead volume is slightly larger (precisely by the volume of the nCh_p, ~30 fL) than for ECS. As an illustration, we use the device to change the IC concentration of Mg^{2+} ($[Mg^{2+}]_i$) while whole-cell *I–V* curves are being obtained. The K_{ir} channel owes its rectifying behavior in part to the blocking of outward current by intracellular Mg^{2+} (which do not block inward current); this "Mg^{2+} block" has previously been artificially removed on cell-free systems ("inside-out" patches) by perfusion with a solution containing 0 mM Mg^{2+} and restored by perfusion with ~1 mM Mg^{2+}.[35] As shown in Fig. 4b, removal of the Mg^{+2} block can be demonstrated with micropipettes using *two different cells* during whole-cell recordings, *e.g.* one *I–V* curve for a cell at $[Mg^{2+}]_i$ = 1 mM and another *I–V* curve for a different cell at $[Mg^{2+}]_i$ = 0 mM (in practice, <1 μM free Mg^{2+}, see Experimental); an outward (positive) current emerges when $[Mg^{2+}]_i$ = 0 mM (partial loss of rectification), presumably because the intracellular Mg^{2+} is depleted by diffusion into the much larger volume of the micropipette. Using our chip, removal of the Mg^{2+} block can be performed *on the same cell*, as shown in Fig. 4c. When the usual ICS (which contains 5 mM Mg^{2+}) is exchanged for a solution containing 0 mM Mg^{2+} (estimated free $[Mg^{2+}]_i$ = 0.19 μM, see Experimental), rectification is also partially removed, albeit over 20 min. Since a free Mg^{2+} ion takes only ~1 s to diffuse through the 30 μm long nCh_p (at the other end of which flow ensures that $[Mg^{2+}]_i$ = 0), total depletion of free intracellular Mg^{2+} should take on the order of seconds. Likely contributors to the delay in Mg^{2+} block removal with our chips are the presence of other cytoplasmic K_{ir} blockers (such as endogenous polyamines[36] or impurities[37]), Mg^{2+} buffering (*i.e.* slow release) by biomolecules (such as ATP and GTP) (see review[38]), the existence of sub-populations of other K_{ir} channels that only rectify current weakly,[39] and migration/trapping of Mg^{2+} into the porous PDMS matrix of the nCh_p and μCh_{out} walls (effectively acting as an additional slow-release buffer).

Summary

We have demonstrated a new PDMS patch clamp chip design that allows high-stability (>10 min) gigaseals to be obtained

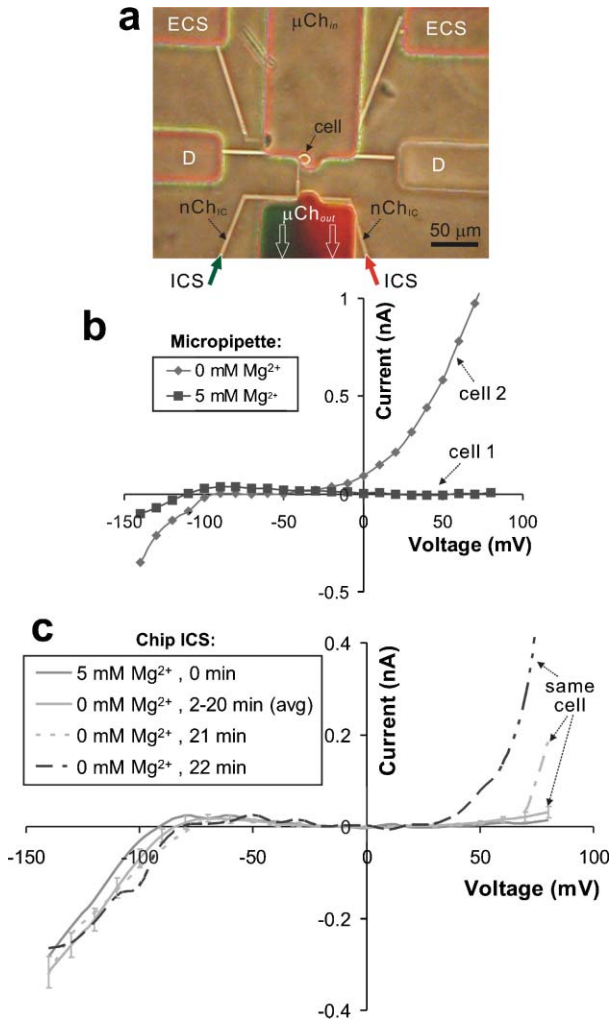

Fig. 4 Microfluidic exchange of the intracellular solution (ICS). (a) Optical micrograph of the device illustrating an ICS exchange with dye solutions. Fluid flows through both nCh_{IC} towards the outlet of μCh_{out} (see arrows indicating flow direction), resulting in a laminar stream boundary that can be steered by changing the flow rates through either nCh_{IC}. (b) Representative steady-state *I–V* curves illustrating micropipette-based Mg^{2+} block removal; the two curves were obtained from two different cells and using two different micropipettes, each loaded with either 0 mM Mg^{2+} (*diamonds*) or 5 mM Mg^{2+} (*circles*). (c) *I–V* curves illustrating chip-based Mg^{2+} block removal; all the curves were obtained from the same cell. Outward current (partial loss of rectification) was substantial only after ~20 min of continuous perfusion with 0 mM Mg^{2+}.

with yields comparable to those obtained with micropipettes (at least for RBL cells). The chip allows for microfluidic exchanges of the extracellular and intracellular solutions. The device is operated essentially like a micropipette but it is superior to a micropipette in many respects: (a) the device is less vibration-sensitive (all recordings were done on the microscope stage without vibration isolation equipment); (b) pickup noise is smaller due to the small volume of fluid (~16 nL) in the device (*i.e.* a Faraday cage is not required for whole-cell recordings); (c) capacitance is smaller because there is a large separation between the intracellular and extracellular solutions (and PDMS is a better dielectric than glass); and (d) micropositioners are not needed (thus automation is foreseeable and setup time is reduced once the chip is fabricated). Fabrication of the device, once the master mold is obtained, is relatively more straightforward and reliable than the fabrication of a micropipette with an expensive pipette-puller. Overall, our detailed analysis of device performance as well as unique perfusion capabilities allows us to conclude that, at the very least in our lab and with RBL cells, the use of devices is *preferable* to the use of micropipettes. In its present design, the device yields similar throughputs to a micropipette, but recent advances in parallel fluidic operation using microvalves[40,41] could presumably be incorporated to multiplex the cell's approach to the microaperture as well as pressure application and signal acquisition for many cells simultaneously. The device presented here is simple enough that it could be easily disseminated to the research community (*e.g.* by shipping the master mold) and inexpensive enough that it could become an affordable commercial product. If the system can be scaled up for parallel operation, it would have an enormous impact in virtually all research involving electrophysiological recordings—including basic neuroscience, drug screening applications, and single-cell sensors, to name a few.

Acknowledgements

This work was supported by NASA (Grant #NAG9-1343), NIH (Grant #RR16302), the Whitaker Foundation (Grant # RG-00-0356), and a UW Center for Nanotechnology Fellowship (C.C.). We are indebted to Dr Kathy Graubard and Dr Lisa Horowitz for insightful discussions and training in general electrophysiology.

References

1 O. P. Hamill, A. Marty, E. Neher, B. Sakmann and F. Sigworth, *Pfluegers Arch.*, 1981, **391**, 85.
2 E. Neher, *Angew. Chem., Int. Ed. Engl.*, 1992, **31**, 824.
3 B. Sakmann, *Science*, 1992, **256**, 503.
4 E. Neher, *Science*, 1992, **256**, 498.
5 B. Hille, *Ion Channels of Excitable Membranes*, 3rd edn, Sinauer Assoc., Sunderland, MA, 2001.
6 N. Fertig, C. Meyer, R. H. Blick, C. Trautmann and J. C. Behrends, *Phys. Rev. E: Stat. Phys., Plasmas, Fluids, Relat. Interdiscip. Top.*, 2001, **64**(4), 040901.
7 N. Fertig, M. Klau, M. George, R. H. Blick and J. C. Behrends, *Appl. Phys. Lett.*, 2002, **81**, 4865.
8 N. Fertig, R. H. Blick and J. C. Behrends, *Biophys. J.*, 2002, **82**, 785.
9 N. Fertig, M. George, M. Klau, C. Meyer, A. Tilke, C. Sobotta, R. H. Blick and J. C. Behrends, *Recept. Channels*, 2003, **9**, 29.
10 J. Xu, A. Guia, D. Rothwarf, M. X. Huang, K. Sithiphong, J. Ouang, G. L. Tao, X. B. Wang and L. Wu, *Assay Drug Dev. Technol.*, 2003, **1**, 675.
11 N. Fertig, A. Tilke, R. H. Blick, J. P. Kotthaus, J. C. Behrends and G. ten Bruggencate, *Appl. Phys. Lett.*, 2000, **77**, 1218.
12 A. Stett, C. Burkhardt, U. Weber, P. van Stiphout and T. Knott, *Recept. Channels*, 2003, **9**, 59.
13 T. Lehnert, M. A. M. Gijs, R. Netzer and U. Bischoff, *Appl. Phys. Lett.*, 2002, **81**, 5063.
14 C. Schmidt, M. Mayer and H. Vogel, *Angew. Chem., Int. Ed.*, 2000, **39**, 3137.
15 R. Pantoja, J. M. Nagarah, D. M. Starace, N. A. Melosh, R. Blunck, F. Bezanilla and J. R. Heath, *Biosens. Bioelectron.*, 2004, **20**, 509.
16 C. Farre, J. Olofsson, J. Pihl, J. Persson and O. Orwar, *Biophys. J.*, 2001, **80**, 338A.

17 K. G. Klemic, J. F. Klemic, M. A. Reed and F. J. Sigworth, *Biosens. Bioelectron.*, 2002, **17**, 597.
18 K. G. Klemic, X. H. Li, J. F. Klemic, M. A. Reed and F. J. Sigworth, *Biophys. J.*, 2002, **82**, 784.
19 K. G. Klemic, J. F. Klemic, M. A. Reed and F. J. Sigworth, *Pfluegers. Arch.*, 2005, **449**, 564.
20 Aviva Biosciences, http://www.avivabio.com.
21 J. Kutchinsky, S. Friis, M. Asmild, R. Taoryski, S. Pedersen, R. K. Vestergaard, R. B. Jacobsen, K. Krzywkowski, T. Ljungstrom, N. Helix, C. B. Sorensen, M. Bech and N. J. Willumsen, *Assay Drug Dev. Technol.*, 2003, **1**, 685.
22 Sophion Bioscience, http://www.sophion.dk/.
23 T. F. Kosar, C. Chen, N. L. Stucky and A. Folch, *J. Biomed. Nanotechnol.*, 2005, **1**, 161.
24 N. L. Stucky, C. Chen, T. F. Kosar and A. Folch, *J. Biomed. Nanotechnol.*, 2005, **1**, 384.
25 J. Seo, C. Ionescu-Zanetti, J. Diamond, R. Lal and L. P. Lee, *Appl. Phys. Lett.*, 2004, **84**, 1973.
26 C. Ionescu-Zanetti, R. M. Shaw, J. G. Seo, Y. N. Jan, L. Y. Jan and L. P. Lee, *Proc. Natl. Acad. Sci. U. S. A.*, 2005, **102**, 9112.
27 A. B. Parekh, A. Fleig and R. Penner, *Cell*, 1997, **89**, 973.
28 Y. N. Xia and G. M. Whitesides, *Angew. Chem., Int. Ed. Engl.*, 1998, **37**, 551.
29 K. T. Brown and D. G. Flaming, *Advanced micropipette techniques for cell physiology*, Wiley, Chichester, West Sussex, UK; New York, USA, 1986.
30 L. F. Horowitz, private communication.
31 N.-T. Nguyen and S. T. Wereley, *Fundamentals and Applications of Microfluidics*, Artech House, Boston, MA, USA, 2002, p. 471.
32 Y. Kubo, T. J. Baldwin, Y. N. Jan and L. Y. Jan, *Nature*, 1993, **362**, 127.
33 B. Sakmann and G. Trube, *J. Physiol. (London)*, 1984, **347**, 641.
34 B. Hille and W. Schwarz, *J. Gen. Physiol.*, 1978, **72**, 409.
35 C. A. Vandenberg, *Proc. Natl. Acad. Sci. U. S. A.*, 1987, **84**, 2560.
36 C. A. Doupnik, N. Davidson and H. A. Lester, *Curr. Opin. Neurobiol.*, 1995, **5**, 268.
37 D. L. Guo and Z. Lu, *J. Gen. Physiol.*, 2002, **120**, 539.
38 D. Luthi, D. Gunzel and J. A. S. McGuigan, *Exp. Physiol.*, 1999, **84**, 231.
39 Z. Lu and R. Mackinnon, *Nature*, 1994, **371**, 243.
40 T. Thorsen, S. J. Maerkl and S. R. Quake, *Science*, 2002, **298**, 580.
41 N. Li, C.-H. Hsu and A. Folch, *Electrophoresis*, 2005, **26**, 3758.